INTERNATIONAL JOURNAL OF CLIMATOLOGY
Int. J. Climatol. **28**: 37–53 (2008)
Published online 1 June 2007 in Wiley InterScience
(www.interscience.wiley.com) DOI: 10.1002/joc.1515

RMetS
ROYAL METEOROLOGICAL SOCIETY

Reconstruction of a 1436-year soil moisture and vegetation water use history based on tree-ring widths from Qilian junipers in northeastern Qaidam Basin, northwestern China

Zhi-Yong Yin,[a]* Xuemei Shao,[b] Ningsheng Qin[c] and Eryuan Liang[d]
[a] *Department of Marine Science and Environmental Studies, University of San Diego, CA 92110, U.S.A*
[b] *Institute of Geographical Science and Natural Resources Research, Chinese Academy of Sciences, Beijing, 100101, P.R. China*
[c] *Qinghai Climate Data Centre, Qinghai Meteorological Bureau, Xining, 810001, P.R. China*
[d] *Institute of Tibetan Plateau Research, Chinese Academy of Sciences, Beijing, 100085, P.R. China*

ABSTRACT: Tree-ring widths have been used widely in studies of environmental changes and reconstructions of past climate. Eleven tree-ring chronologies of approximately 800–1500 years long were developed from Qilian junipers (*Sabina przewalskii Kom.*) for northeastern Qaidam Basin, along the margin of the Qinghai–Tibetan Plateau. Previous studies have revealed that water usage stress is the most limiting factor for tree growth in the study region. To evaluate the impact of the combined effects of temperature and precipitation changes over time, we performed water balance modelling using 1955–2002 meteorological data. We found that the tree-ring widths were strongly correlated with variables representing soil moisture conditions obtained from the water balance model. Specifically we considered actual evapotranspiration (AE) to represent the combined effect of water use demand and moisture availability, deficit as the difference between potential evapotranspiration (PE) and AE to represent the severity of water use stress, and relative soil moisture as the measure of moisture availability. For certain individual monthly and seasonal combinations, the tree-ring chronologies explained up to 80% of the variation in the soil moisture variables in regression analysis, indicating very good potential for reconstruction of regional soil moisture conditions in the past. These soil moisture variables outperformed precipitation and Palmer's drought severity index in most cases. We reconstructed the soil moisture conditions from 566 AD to 2001, which revealed major dry and wet periods and a general trend toward a wetter condition during the most recent 300 years. By comparing with other proxies in the region, we concluded that the moisture conditions reconstructed from tree-ring widths very well reflected the climate variability at the interannual and interdecadal scales. Copyright © 2007 Royal Meteorological Society

KEY WORDS dendroclimatology; water balance modelling; reconstruction of soil moisture condition

Received 14 December 2005; Revised 23 January 2007; Accepted 4 February 2007

1. Introduction

Anthropogenic climate changes since the Industrial Revolution have attracted much attention in recent years. One often debated question is whether the magnitude of the climate change has exceeded the range of natural variability of the climate system (Folland *et al*., 2001). Therefore, there is the need to study climate during the historical time using high resolution proxies for patterns of the natural variability in the past and to evaluate the potential implications of climate changes for the future (Bradley, 2000). Previous studies based on a variety of proxies, such as tree rings, pollens, speleothems, and ice cores, have revealed that significant cooling and warming episodes existed since the dawn of civilization (Lamb, 1995; Thompson *et al*., 1986; Thompson *et al*., 1993; Hughes *et al*., 1999; Bradley *et al*., 2003). Some of these events occurred at similar temporal scales as compared to the more recent global warming and, therefore, may provide insights into the mechanisms of climatic changes, the scope or magnitude of natural variability of the climate system, the responses of ecosystems, as well as the adaptive strategies of the human society to cope with these relatively rapid changes in climate.

Since the growth of trees under temperate climates is closely related to the heat and moisture availability of any given year, tree rings have been used widely in reconstructions of past environments. By measuring tree-ring widths, information on growing conditions in the past can be extracted and used to reconstruct variation patterns of various climatic variables (Fritts, 1976; Bradley, 1999; Briffa and Osborn, 1999). Compared with other proxies of climate, tree rings offer the advantage of high temporal resolution at the interannual scale. Several recent studies reconstructed long records of climatic variability, focusing on the past 2500 years, of temperature and precipitation in the Qaidam Basin of northwestern China, along the northeastern margin of the Tibetan Plateau (e.g. Zhang *et al*., 2003a; Sheppard *et al*., 2004; Shao *et al*.,

* Correspondence to: Zhi-Yong Yin, Department of Marine Science and Environmental Studies, University of San Diego, CA 92110, U.S.A.
E-mail: zyin@sandiego.edu

2005). Fluctuations of climate in this region may have caused the thriving and destruction of human settlements during the historical times (Yang *et al*., 2004).

In arid and semi-arid regions, soil moisture is the most direct controlling factor of tree growth. Owing to the lack of long records of field measurements and great spatial variation in soil properties, soil moisture has not been considered by most dendroclimatologists as a common metric in reconstruction efforts. However, streamflow has been reconstructed using tree rings (Woodhouse, 2001; Meko and Woodhouse, 2005), which can be considered as the residual between precipitation, evapotranspiration loss, and soil storage fluctuation on an annual basis. In a few studies, water balance models were used directly to examine the relationships between tree rings and the simulated vegetation water use and soil moisture conditions (LeBlanc and Terrella, 2001; Robertson *et al*., 1990; Piutti and Cescatti, 1997). There have also been studies relating tree rings to the Palmer's drought severity index (PDSI), which is based on water balance calculations for a generic soil (e.g. Puckett, 1981; Meko *et al*., 1993; Cook *et al*., 2004; Leavitt, 2002; Sheppard *et al*., 2002; Buckley *et al*., 2004; Hidalgo, 2004; Zhang *et al*., 2004a; Taylor and Beaty, 2005). In an effort to reconstruct the 1000 year precipitation history in northeastern Qaidam Basin, Shao *et al*. (2005) found strong correlations between tree-ring widths and a variety of climate variables, including June maximum and mean temperatures, pan evaporation rate, relative humidity, and monthly mean vapour pressure, which are all directly or indirectly related to the water balance process. These relationships indicated the potential of using tree rings to reconstruct the water balance process in this region.

The main purpose of this study is to reconstruct the history of regional soil moisture conditions in northeastern Qaidam Basin based on tree-ring widths. Previous studies have revealed that tree-ring width was positively correlated to early summer precipitation but negatively correlated to temperature during the same time (Shao *et al*., 2005; Tardif *et al*., 2001), similar to the earlier findings in the western United States (Fritts, 1976) and suggesting soil moisture availability as the limiting factor of tree growth. We developed tree-ring chronologies over 1400 years long, which included several important climatic events, such as the medieval warming, Little Ice Age, and the post-industrial period warming. Studying how soil moisture conditions responded to climate variations during these events may improve our understanding to the impact of future climate changes on water resources availability and surface processes in the study region. In this study, variables representing soil moisture and vegetation water use conditions were obtained from water balance modelling. Water balance models have been widely used in assessing the regional impact of climate changes and vegetation/crop responses for future scenarios (e.g. Hulme *et al*., 1992; Kenny and Harrison, 1992; Feddema, 1998, 1999; Hodny and Mather, 1999; Leathers *et al*., 2000; Sharma *et al*., 2000; Shabalova *et al*., 2003), and many of these studies were based on the Thornthwaite–Mather method (Thornthwaite and Mather, 1957). Water balance modelling is the basis of hydrological modelling, consisting of moisture input, output, and storage change of the soil-vegetation continuum system to

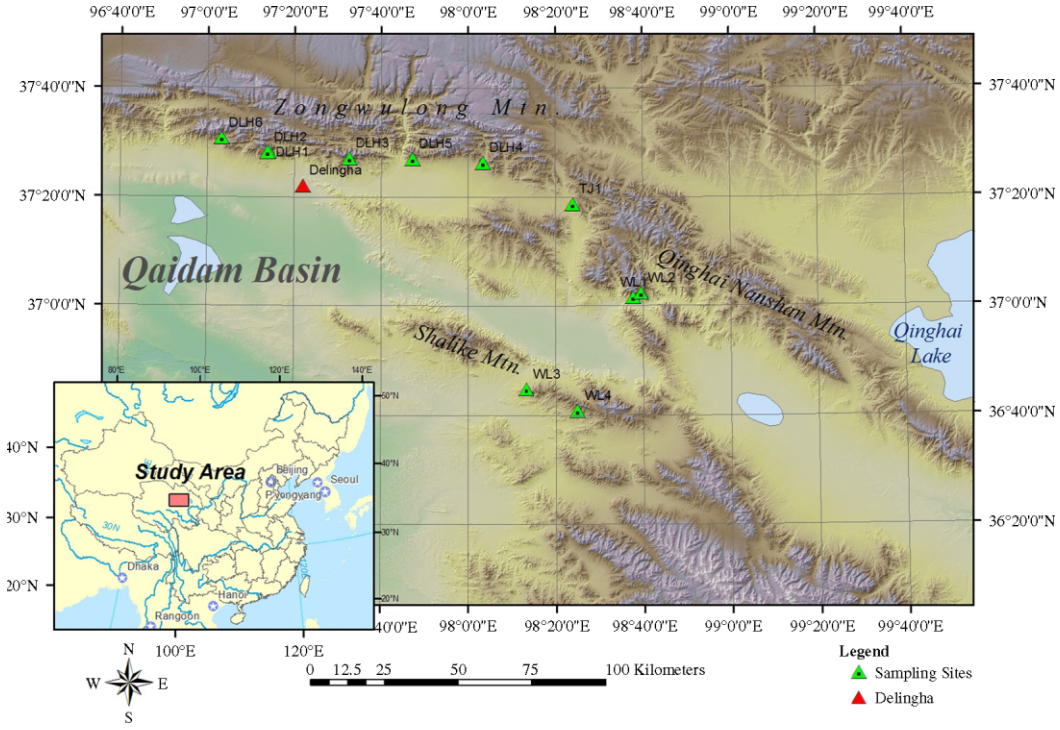

Figure 1. Study area and sampling sites. Delingha is the city with the weather station, whose data were used in reconstruction. This figure is available in colour online at www.interscience.wiley.com/ijoc

DOI: 10.1002/joc

Figure 2. Sparse junipers on south-facing slopes at WL1 (a) and dense spruce forest near the valley head at WL2 (b). This figure is available in colour online at www.interscience.wiley.com/ijoc

simulate the soil moisture depletion by evapotranspiration and replenishment by precipitation (Mather, 1978).

2. Study area and the tree-ring sampling sites

The study area is located in the northeastern part of the Qaidam Basin, mainly in Delingha and Wulan Counties of Qinghai Province in northwestern China (Figure 1), along the northeastern margin of the Qinghai–Tibetan Plateau. The city of Delingha is located on the margin of alluvial fans with elevations between 2900 and 3000 m above mean sea level (a.m.s.l.), while the mountains in the region can reach 4400 m or higher. The annual mean temperature is 3.7 °C, with a mean January temperature of −11.9 °C and a mean July temperature of 16.7 °C at the Delingha weather station. The annual total precipitation is less than 200 mm in the region, declining from east to west and with up to 80% falling from May to September. The region is characterized by a landscape of desert steppe (Zheng, 1996) with natural vegetation consisted of various desert and dry grassland plants. Less arid climate, however, appears in the mountainous areas. Coniferous trees composed of Qilian juniper (*Sabina przewalskii Kom.)*, an endemic species of the region, and Qinghai spruce (*Picea crassifolia*) are found in the elevation zone between 3450 m and 4200 m a.m.s.l. (Figure 2), which receives more precipitation due to orographic effect (Du and Sun, 1990). The junipers are mostly seen on steep south-facing hillslopes with thin and stony soils. Zongwulong Mountain is found to be the westernmost limit

DOI: 10.1002/joc

of Qilian junipers' natural range in the arid area (Wang, 1993).

Since 1998, 1050 tree-ring increment cores have been extracted from 493 living trees at Zongwulong, Shalike and Qinghai Nanshan mountains (Figure 1) in the northeastern part of Qaidam Basin. The 11 sampling sites (DLH1–6, TJ1, and WL1–4) are located to the north of the Dulan Chronology site (Zhang *et al*., 2003a; Tarasov *et al*., 2003). Table I presents the details of these sites and the sample depths. Soils at these sites developed poorly from loess with a general thickness of 20–50 cm on gentle slopes, but shallower on steep and heavily eroded slopes. The only exception is the soils at TJ1, which are sandy and thick with the gentlest slopes among all the sites. Mixed forests of Qinghai spruce and Qilian juniper are present at the two eastern sites, WL1 and WL2 (Figure 2), while Qilian juniper is the only dominant species at the other nine sites.

The canopy coverage is generally low with trees ranging from 3 to 6 m high. Since the percentage of missing rings is high for Qilian junipers growing in this arid region (Shao *et al*., 2003), we collected large samples at several sites from trees with a variety of ages and in different microenvironments (Table I). Sometimes, more than two cores were taken from a single tree. Such sampling strategies were helpful in cross-dating the ring widths and reducing the possibility that all collected specimens could miss the same ring for any given year at a site.

3. Data and methods

Details of the methods of tree-ring sampling, data processing, and cross-dating can be found in Shao *et al*. (2005). The chronologies used in this study are extensions of those reported in the earlier study after more samples were collected from the same sites in the study area, adding more than 400 years to the regional chronology. Correlation analysis was used to investigate the relationship between tree-ring widths and soil moisture variables. Then regression analysis was employed to derive the transfer equations for reconstruction.

Daily precipitation, temperature, and pan evaporation data during 1955–2002, and soil moisture measured three times a month (8th, 18th, and 28th of the month from May to September) during 1981–2002 at Delingha were obtained from the Climate Centre of Qinghai Meteorological Bureau. Daily precipitation and temperature data were used as the water balance modelling input, while the evaporation and soil moisture observations, and tree ring width data during 1955–2002 were used to cross-check the model results to ensure that model performance was acceptable.

Besides soil moisture calculated using a daily budgeting procedure, the water balance modelling process also produces several parameters that can be related to tree growth. Potential evapotranspiration (PE) is defined as the combined evaporation and transpiration from an extensive well-watered grass-type vegetation surface, representing the demand of vegetation water use under a specific atmospheric condition (Rosenberg *et al*., 1983). Daily PE values were calculated following the original Thornthwaite method using daily mean temperature data (Thornthwaite and Mather, 1957). Since the Thornthwaite method is based only on daily or monthly mean temperature as the input, it would be easy to assess the impact of long-term temperature changes. For days with mean temperature below zero, a daily PE value of 0.01 mm was assigned for evaporation loss. This modification is small enough not to create any major deviations from the original method, but in the mean time it also eliminates days of zero evaporation loss for the ease of data transformation (e.g. logarithmic transformation) in analysis. Actual evapotranspiration (AE) combines the effect of atmospheric demand (through PE) with that of moisture availability from precipitation and soil storage. It has been found to be closely related to the intensity of regional biological activities (Meentemeyer *et al*., 1985). Deficit (DEF) is defined as the difference between the PE and AE. It is a measure of

Table I. Information of the sampling sites in northeastern Qaidam Basin.

I.D.	Latitude (N)	Longitude (E)	Elevation (m a.s.l.)	Slope Aspect	Slope Angle (°)	Sample Depth (trees/cores)
DLH1	37°28′14″	97°14′06″	3730	WNW	38	31/61
DLH2	37°28′05″	97°13′44″	3780	SSW	22	34/73
DLH3	37°27′05″	97°32′33″	3920	SSW	20	79/168
DLH4	37°26′19″	98°03′23″	3800	S	13	67/144
DLH5	37°26′59″	97°47′07″	3700	S	31	67/146
DLH6	37°30′46″	97°03′20″	3780	S	30	29/67
TJ1	37°18′43″	98°23′56″	3500	SSW	10	29/58
WL1	37°01′33″	98°37′46″	3700	S	38	20/40
WL2	37°02′17″	98°39′34″	3700	SE	38	44/91
WL3	36°44′52″	98°13′16″	3720	NNW	19	43/99
WL4	36°40′46″	98°24′58″	3700	SSW	18	50/103

[1] DLH: Delingha; TJ: Tianjun; WL: Wulan

DOI: 10.1002/joc

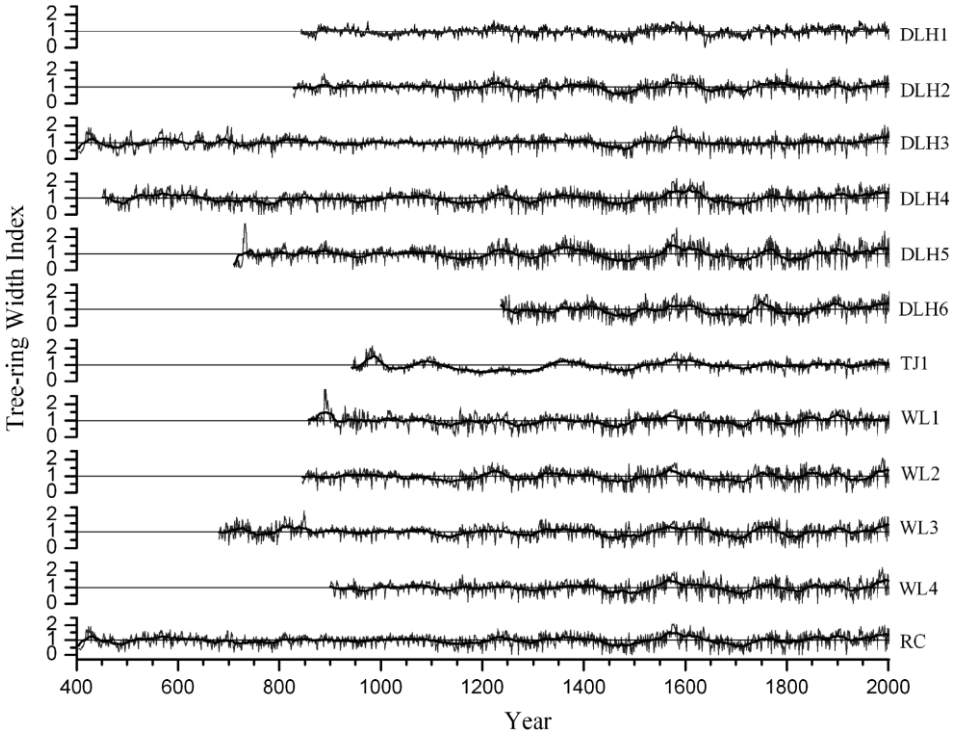

Figure 3. Chronologies of ring-width from the 11 sampling sites in the study area and the regional chronology (RC).

Table II. Summary statistics for the 11 chronologies and the regional chronology (RC), and the results of common interval analysis.

I.D.	Standard chronology					Common interval (1401–1600) analysis					
	Trees/ cores	Mean sensitivity	Std. dev.	Auto corr.	Mean length	Trees/ Cores	Mean corr.	Signal/ noise	APC[1]	PCA1[2] (%)	SSS[3] >0.85
Long chronologies for climate reconstruction											
DLH1	22/41	0.24	0.26	0.45	573.4	19/30	0.49	17.7	0.95	51.8	1082(7)[4]
DLH2	24/43	0.33	0.33	0.38	580.2	17/29	0.54	19.5	0.95	57.2	945(5)
DLH3	22/43	0.31	0.32	0.40	821.1	20/38	0.58	26.3	0.96	59.2	898(5)
DLH4	22/44	0.44	0.40	0.37	698.7	19/33	0.58	25.6	0.96	60.2	588(5)
DLH5	30/55	0.52	0.47	0.40	674.2	23/36	0.69	50.1	0.98	71.5	747(3)
DLH6	28/55	0.50	0.44	0.38	505.2	10/19	0.55	11.7	0.92	58.5	1309(5)
TJ	27/51	0.22	0.30	0.66	505.2	9/16	0.63	14.3	0.94	66.1	1232(4)
WL1	20/39	0.39	0.38	0.43	564.4	10/17	0.55	11.7	0.92	59.1	1042(5)
WL2	24/48	0.42	0.38	0.38	624.9	22/37	0.63	37.2	0.97	65.1	914(4)
WL3	23/46	0.37	0.37	0.40	797.7	18/35	0.54	20.4	0.95	56.8	835(5)
WL4	25/44	0.42	0.39	0.37	786.0	23/37	0.65	40.9	0.98	66.8	971(4)
RC	43/80	0.38	0.37	0.40	802.9	34/55	0.56	42.3	0.98	57.5	566(5)

[1] Agreement with population chronology (APC) (Wigley *et al*., 1984; Cook and Kairiukstis 1990).
[2] Variance explained by the first principal component (PCA1).
[3] Subsample signal strength (SSS) (Wigley *et al*., 1984; Cook and Kairiukstis 1990).
[4]The year and the number of trees required to attain an SSS of 0.85.

the unmet demand of vegetation water usage and can be treated as an indicator of water shortage or drought conditions.

In this study, a simple soil moisture depletion function was used for the ease of computation. First, the demand for soil water is calculated as the difference between daily PE and precipitation (P) for days of PE>P. The amount to be extracted from the soil depends on the relative soil moisture (RSM) (RSM= soil moisture/field capacity) of the previous day. The proportion of the unmet PE that can be satisfied by soil water was determined as:

$$C_t = RSM_{t-1}$$

where RSM_{t-1} is the relative soil moisture value of the previous day. In other words, as RSM decreases due to

DOI: 10.1002/joc

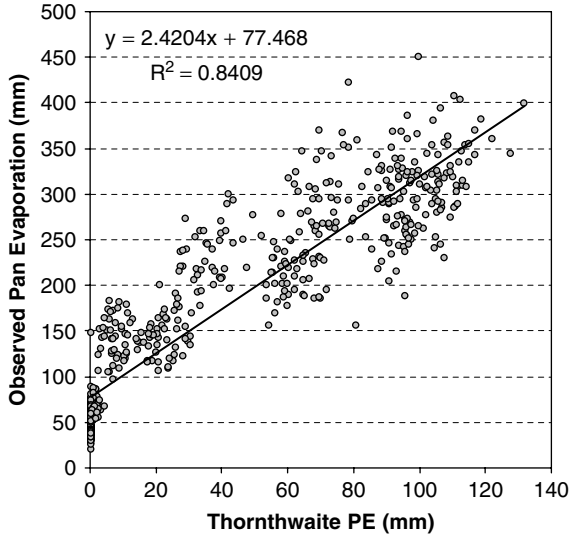

Figure 4. A comparison between the monthly total Thornthwaite potential evapotranspiration and pan evaporation observed at Delingha during 1955–2002.

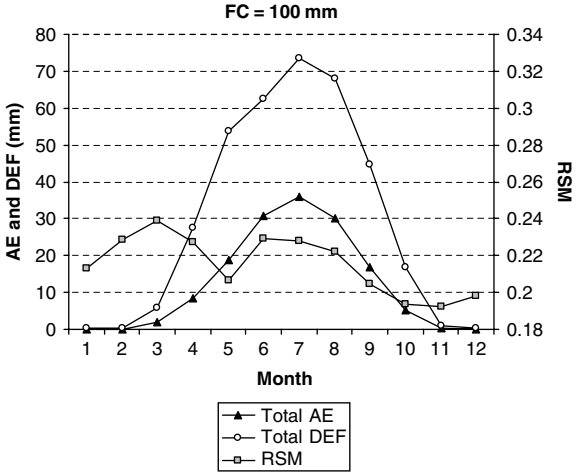

Figure 5. Seasonal variation pattern of water balance variables based on long-term means during 1955–2002.

soil moisture depletion, the capability to further withdraw water from the soil decreases linearly as RSM continues to lower and it becomes more and more difficult to extract soil moisture for vegetation water use. Then AE of day t is calculated as $AE_t = C_t \times PE'_t + P_t$, where PE'_t is the unmet portion of PE_t, P_t is the precipitation amount of that day, and $C_t \times PE'_t$ is the amount of water extracted from the soil unless soil moisture reaches zero.

After daily values were simulated by the model, monthly values were summarized to get the total AE, total DEF, and mean monthly RSM. We constructed various bi-monthly, seasonal, and annual composites of the soil moisture variables. Of the multitude of variables we examined, we selected those most promising for reconstruction of the past moisture conditions.

4. Results and discussion

4.1. Developing ring-width chronologies

For Qilian junipers growing in arid regions, cross-dating may run into problems due to missing rings associated with extremely slow growth rates of this species and harsh conditions during severe droughts. The cores with missing rings were verified by cross-dating the ring patterns with other cores/sections that did not have missing rings. The accuracy of cross-dating and measurements was further checked using the COFECHA program (Holmes, 1983) with the default parameters. In order to enhance the common signals and long-term trends, we selected samples from old trees in chronology development. Among the 11 sites, only DLH6 yielded cores less than 1000 years in length, and the longest sample was obtained at DLH3 going back to 404 AD. We compared our chronologies with an archaeological ring-width chronology and the Dulan chronology (Zhang *et al*., 2003a; Kang *et al*., 1997; Tarasov *et al*., 2003; Sheppard

Table III. Correlation coefficients of the simulated soil moisture values with different field capacity values (10–200 mm) against the observed values at Delingha station for 8th, 18th, and 28th of each month during 1980–2002.

FC		Soil Moisture Measured at				
		10 cm	20 cm	30 cm	40 cm	50 cm
10 mm	Correlation	**0.248***	**0.243**	**0.173**	0.071	0.100
	Sig. (2-tailed)	0.000	0.000	0.004	0.257	0.120
	N	298	282	268	255	241
30 mm	Correlation	**0.282**	**0.328**	**0.294**	***0.209***	**0.195**
	Sig. (2-tailed)	0.000	0.000	0.000	0.001	0.002
	N	298	282	268	255	241
100 mm	Correlation	**0.315**	**0.373**	**0.381**	**0.304**	**0.289**
	Sig. (2-tailed)	0.000	0.000	0.000	0.000	0.000
	N	298	282	268	255	241
200 mm	Correlation	**0.310**	**0.375**	**0.408**	**0.305**	**0.295**
	Sig. (2-tailed)	0.000	0.000	0.000	0.000	0.000
	N	298	282	268	255	241

* Boldface numbers with underscores indicate statistical significance of 0.01.

DOI: 10.1002/joc

et al., 2004). The comparisom revealed that dating trees from the arid and semi-arid regions can be very difficult because of the missing rings and replications and comparisons between chronologies are extremely beneficial to improve the accuracy of chronologies.

According to chronological statistics in Table II, the ring-width chronology at DLH5 is of the best quality, with the highest mean correlation among radii, signal-to-noise ratio (Fritts, 1976), expressed population signal (Wigley *et al*., 1984), and the variance in the first eigenvector. It also contains the most year-to-year variability, as indicated by mean sensitivity (Fritts, 1976). In contrast, the chronology at TJ1 has the lowest mean sensitivity and the highest first-order autocorrelation, indicating low levels of year-to-year variation. The mean sensitivity of our samples varied between 0.35 and 0.63, suggesting that the junipers are indeed sensitive to environmental variability (Fritts, 1976). The statistics of the expressed population signal ranging from 0.86 to 0.98 implies that Qilian juniper in the study area is a highly suitable species for dendroclimatological studies since a value of 0.85 is considered as the acceptable threshold by many scholars (Wigley *et al*., 1984; Cook and Kairiukstis, 1990). The tree-ring chronologies have a high degree of agreement in low-frequency as well as in high-frequency variations (Figure 3), even though the sampling sites are distributed over a region almost 140 km across.

Given the strong correlations among the chronologies at different sites, we developed a regional chronology (RC) for the study region (Figure 3). Samples with ages over 1050 years long and of strong correlations with the mean series from each site were selected for this purpose. The sample depth of the RC is seven cores from five trees in 600 AD, nine cores from seven trees in 700 AD, 22 cores from 16 trees in 800 AD, and then it increases to more than 50 cores out of 36 trees in 900 AD. The quality of the tree-ring chronologies normally shows a gradual decay duo to the diminishing replication of samples going back in time. In general, the statistics of subsample signal strength (Wigley *et al*., 1984) are often used when making the decision to truncate a chronology (Cook and Kairiukstis, 1990; Hughes *et al*., 1999; Kirchhefer, 2001). In our study, the subsample signal strength reached 0.85 in 566 AD when there were six cores from five trees in this chronology, suggesting that the chronology should be truncated at this year for the purpose of climate reconstruction with relatively high confidence.

4.2. Water balance modeling

Figure 4 shows the monthly total PE calculated using the Thornthwaite method plotted against the observed evaporation data from a small evaporation pan (20 cm diameter and 10 cm depth) at the Delingha weather station. It can be concluded that the Thornthwaite PE should be able capture the overall pattern of the evapotranspiration demand in the study area and produce reasonable results in water balance modelling, as the simulated PE explained more than 84% of the variance in the observed evaporation data. It is not surprising that the model calculated PE values are much lower than the observed evaporation data since the small size of the evaporation pan would cause significant overestimates of PE in an arid environment (Dunne and Leopold, 1978).

We performed multiple runs of the water balance model using different soil field capacity values (10 mm to 200 mm). Although the monitored soil moisture data are available for part of the study period, a comparison could only confirm the general range of soil moisture variation during the growing season since the observed data were not continuous. Table III contains the correlation coefficients between the simulated soil moisture using various field capacity values from 10 to 200 mm and the observed soil moisture values. There is a general trend of higher correlation with increasing field capacity values, suggesting that the soil column monitored at the weather station must be fairly thick. Low correlations

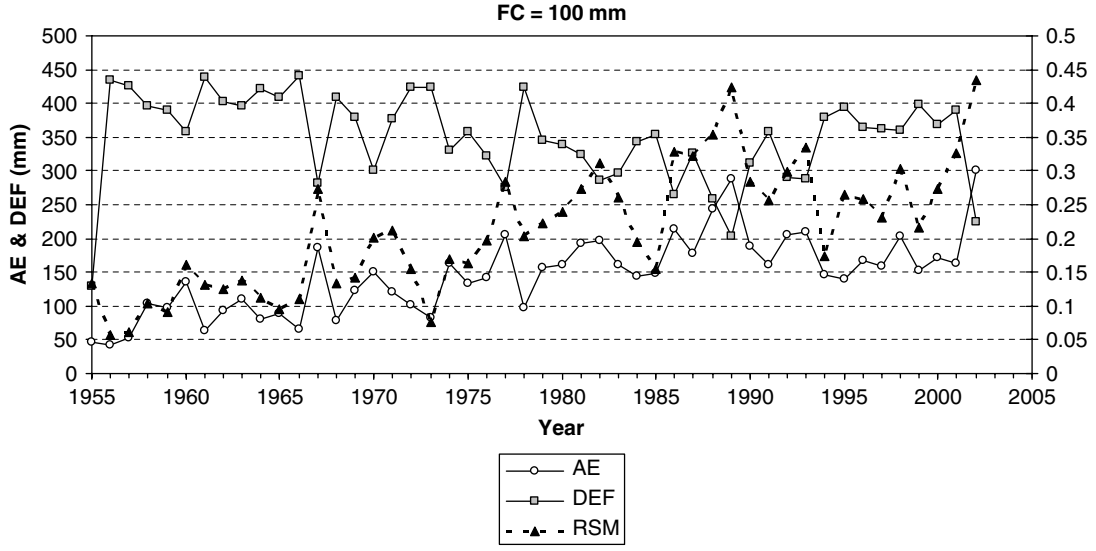

Figure 6. Interannual variation patterns of the water balance variables during 1955–2002.

DOI: 10.1002/joc

between the simulated and observed soil moisture values were probably caused by the monitoring schedule that did not include the full range of annual variation of soil moisture in a continuous way. However, strong correlations between the simulated soil moisture variables and tree growth (see below) suggest that the simulated values should be reasonable to reflect temporal variation patterns of the moisture conditions. Here we present the results of the model run for a field capacity of 100 mm, probably best representing the regional moisture variation pattern or representing the moisture conditions of thick soils on gentle slopes or plains within the region. Figure 5 presents the long-term mean monthly values of the water balance modelling results. It shows that in the study area, precipitation and high demand of water usage usually occur at the same time, a common feature of the monsoon climate. However, precipitation is much lower than PE, introducing high levels of deficit during the warm season. During the winter months, PE is close to zero due to sub-zero temperatures. The relative soil moisture reaches the highest value in early spring and then gradually decreases during the warm season. At the onset of the raining season (May), there is a minor reversal of the moisture depletion trend, but warm temperatures in the summer would create high water use demands and continue the soil moisture depletion process.

4.3. Relationships between tree-ring widths and soil moisture conditions

The water balance variables displayed well-defined seasonal cycles as well as interannual variations. For example, the early 1960s was a period of droughts with low AE and RSM, but high DEF values. It was followed by a period of high variability in the 1970s (Figure 6). There was an overall trend to a wetter condition during the study period as indicated by the increasing trends of AE and RSM.

We used the chronology at DLH5 in the correlation analysis to illustrate the relationships between tree-ring widths and the simulated soil moisture variables (Table IV) because this chronology has the best quality among the sampling sites (Table II). The month with the strongest correlations is June, followed by May, suggesting the significance of moisture conditions during these months to tree growth in the area. Among the water balance variables examined in this study, DEF produced the highest correlation coefficient (–0.815 for June). There were also significant correlations for previous year's summer and fall months, which may indicate the cumulative effect of soil moisture conditions on vegetation growth. To evaluate the strength of the relationships between the soil moisture variables and the tree ring chronologies at different sites, we also calculated correlation coefficients for May, June, July, calendar year (JAN–DEC), annual (pJUL–JUN), and growing season (APR–JUL) (Table V). The month with the highest correlation coefficients is June, followed by the period of April–July, and the period from July previous year to current June.

Table IV. Correlation coefficients and statistical significance between tree-ring widths at DLH5 and the soil moisture variables during the calibration period 1955–2002. Boldface numbers indicate statistical significance of 0.05; those with underscores indicate statistical significance of 0.01.

	AE	DEF	RSM
pJUL*	0.207	−0.171	0.203
Sig. (2-tailed)	0.168	0.255	0.176
pAUG	**0.351**	**−0.357**	0.249
Sig. (2-tailed)	0.016	0.014	0.091
pSEP	**0.359**	**−0.323**	**0.375**
Sig. (2-tailed)	0.013	0.027	0.009
pOCT	0.249	0.136	**0.288**
Sig. (2-tailed)	0.091	0.363	0.050
pNOV	0.147	0.037	0.267
Sig. (2-tailed)	0.324	0.807	0.070
pDEC	0.224	−0.206	0.215
Sig. (2-tailed)	0.129	0.165	0.146
JAN	**0.337**	−0.257	0.279
Sig. (2-tailed)	0.021	0.082	0.057
FEB	−0.082	−0.277	**0.330**
Sig. (2-tailed)	0.582	0.059	0.024
MAR	**0.363**	−0.007	**0.348**
Sig. (2-tailed)	0.012	0.962	0.017
APR	**0.348**	**−0.311**	**0.392**
Sig. (2-tailed)	0.016	0.033	0.006
MAY	**0.512**	**−0.504**	**0.497**
Sig. (2-tailed)	0.000	0.000	0.000
JUN	**0.740**	**−0.815**	**0.682**
Sig. (2-tailed)	0.000	0.000	0.000
JUL	**0.518**	**−0.433**	**0.485**
Sig. (2-tailed)	0.000	0.002	0.001
AUG	0.164	−0.141	0.184
Sig. (2-tailed)	0.266	0.339	0.209
SEP	−0.035	0.046	−0.014
Sig. (2-tailed)	0.813	0.756	0.924
Annual (JAN–DEC)	**0.529**	**−0.583**	**0.401**
Sig. (2-tailed)	0.000	0.000	0.005
Annual (pJUL–JUN)*	**0.598**	**−0.667**	**0.449**
Sig. (2-tailed)	0.000	0.000	0.002
Growing Season (APR–JUL)	**0.655**	**−0.700**	**0.599**
Sig. (2-tailed)	0.000	0.000	0.000

* pJUL – pDEC are months in the previous year.

4.4. Reconstruction of soil moisture conditions in the past

We employed multiple regression analysis to reconstruct soil moisture conditions using individual tree-ring chronologies at different sites as the independent variables. Trees growing in the same region but at different locations may have variable responses to environmental variations of different nature and frequencies (Hughes and Funkhouser, 2003). Owing to the variation of site conditions in topography, geographic location, soil, and microclimate, each chronology may represent a specific aspect of the regional soil moisture condition. It may also be possible that the trees at different sites had variable sensitivity levels to the same

DOI: 10.1002/joc

Table V. Correlation coefficients between soil moisture variables and tree ring chronologies at different sites.

Moisture Variables	Sites	MAY	JUN	JUL	CALENDAR JAN–DEC	ANNUAL pJUL–JUN*	APR-JUL
AE	DLH1	0.433	0.576	0.443	0.454	0.598	0.552
AE	DLH2	0.450	0.682	0.381	0.424	0.624	0.576
AE	DLH3	0.468	0.696	0.391	0.438	0.561	0.575
AE	DLH4	0.456	0.651	0.385	0.400	0.484	0.537
AE	DLH5	0.512	0.740	0.518	0.529	0.598	0.655
AE	DLH6	0.548	0.768	0.526	0.524	0.576	0.676
AE	TJ1	0.387	0.514	0.274	0.267	0.488	0.414
AE	WL1	0.325	0.496	0.310	0.289	0.387	0.406
AE	WL2	0.620	0.641	0.533	0.609	0.677	0.673
AE	WL3	0.621	0.757	0.461	0.523	0.658	0.688
AE	WL4	0.598	0.704	0.539	0.562	0.626	0.679
AE	RC	0.555	0.727	0.458	0.492	0.602	0.632
DEF	DLH1	−0.405	−0.632	−0.416	−0.548	−0.680	−0.615
DEF	DLH2	−0.379	−0.715	−0.294	−0.423	−0.627	−0.563
DEF	DLH3	−0.464	−0.751	−0.275	−0.431	−0.565	−0.572
DEF	DLH4	−0.501	−0.742	−0.332	−0.493	−0.573	−0.614
DEF	DLH5	−0.504	−0.815	−0.433	−0.583	−0.667	−0.700
DEF	DLH6	−0.505	−0.818	−0.433	−0.547	−0.590	−0.679
DEF	TJ1	−0.433	−0.616	−0.251	−0.401	−0.631	−0.526
DEF	WL1	−0.397	−0.606	−0.277	−0.412	−0.479	−0.503
DEF	WL2	−0.614	−0.672	−0.472	−0.666	−0.748	−0.740
DEF	WL3	−0.584	−0.782	−0.345	−0.555	−0.684	−0.700
DEF	WL4	−0.632	−0.763	−0.474	−0.658	−0.731	−0.764
DEF	RC	−0.586	−0.802	−0.381	−0.579	−0.688	−0.705
RSM	DLH1	0.443	0.533	0.398	0.335	0.446	0.526
RSM	DLH2	0.411	0.594	0.361	0.322	0.451	0.505
RSM	DLH3	0.426	0.615	0.389	0.313	0.388	0.508
RSM	DLH4	0.407	0.611	0.377	0.284	0.345	0.483
RSM	DLH5	0.497	0.682	0.485	0.401	0.449	0.599
RSM	DLH6	0.495	0.716	0.545	0.422	0.452	0.608
RSM	TJ1	0.355	0.478	0.257	0.192	0.359	0.387
RSM	WL1	0.299	0.432	0.289	0.160	0.256	0.349
RSM	WL2	0.631	0.634	0.451	0.504	0.543	0.657
RSM	WL3	0.587	0.703	0.418	0.444	0.514	0.639
RSM	WL4	0.585	0.659	0.508	0.449	0.472	0.634
RSM	RC	0.531	0.679	0.430	0.381	0.447	0.588

* pJUL – DEC is the period from July of previous year to current June.

regional environmental condition. As the result, a combination of the chronologies with different weights (in the form of regression coefficients) may best predict the regional moisture conditions. As indicated by the results of correlation analysis (Tables IV and V), soil moisture conditions have lagged effects on the growth of trees in the following years. Therefore, in regression analysis, we included the ring widths lagging up to 2 years as the independent variables. First we used stepwise regression to allow independent variables to enter the model at the significance level of 0.15. Then we used two additional criteria to eliminate any variable in the equation, which did not meet the requirements. The first criterion (with a higher priority) is that all variables in the final equation should represent the correct relationship, as indicated by the sign of the regression coefficient. The only exception allowed was for the chronology of WL1, which will be discussed in greater detail in the following. The second criterion is that all variables in the final equation must have a statistical significance of 0.05 or better. For any variable that did not meet the criteria, it was eliminated from the pool of independent variables before the stepwise procedure was repeated. In addition, we also used the backward regression procedure to verify the stepwise results. We excluded the chronologies at DLH6 for its short length and TJ1 for its insensitivity to environmental variability.

Table VI contains the final regression equations for selected monthly, bi-monthly, seasonal, and annual soil moisture conditions. In most cases, ring widths explained more variance in AE and DEF than that in RSM. The best performance is for May–June AE with an adjusted R^2 of 0.80. As a comparison, the tree ring chronologies explained up to 39.2% of the variance in precipitation for individual months, up to 58.7% for bi-monthly periods,

DOI: 10.1002/joc

Table VI. Transfer functions for reconstruction. All results are based on model output for field capacity values of 100 mm.

Dependent Var.	R	R^2	R_a^2	F	Transfer Functions
AE 4	0.740	0.548	0.501	11.806	$-7.71 + 0.0424$WL3_1 $+ 0.0960$DLH1 $+ 0.0711$WL3$_2$ $- 0.0815$WL1_2
AE 5	0.834	0.696	0.673	30.512	$-16.5 + 0.136$WL3 $+ 0.09469$WL2_1 $+ 0.06044$WL3_2
AE 6	0.877	0.768	0.751	44.220	$-31.3 + 0.260$DLH5 $+ 0.144$WL3_2 $+ 0.090$DLH4_1
AE 7	0.640	0.409	0.381	14.539	$8.62 + 0.115$WL2_1 $+ 0.112$WL4
AE 4–5	0.832	0.691	0.660	21.853	$-11.6 + 0.104$WL2_1 $+ 0.190$WL3_2 $+ 0.175$WL3 $- 0.180$WL1_2
AE 5–6	0.910	0.828	0.800	29.587	$-44.8 + 0.162$WL2_1 $+ 0.107$WL3_2 $- 0.389$WL1 $+ 0.280$DLH4 $+ 0.249$DLH1 $+ 0.317$WL3
AE 6–7	0.824	0.678	0.654	28.102	$-20.8 + 0.205$WL2_1 $+ 0.342$DLH5 $+ 0.165$WL3_2
AE 4–6	0.894	0.799	0.772	30.201	$-27.5 + 0.310$WL3 $+ 0.164$WL2_1 $+ 0.170$WL3_2 $+ 0.313$DLH5 $- 0.315$WL1
AE 5–7	0.884	0.781	0.753	27.171	$-14.1 + 0.254$WL4 $+ 0.234$WL2_1 $- 0.423$WL1 $+ 0.193$WL3_2 $+ 0.475$DLH5
AE 4–7	0.901	0.811	0.775	22.111	$-37.1 + 0.415$WL3 $+ 0.286$WL2_1 $+ 0.435$DLH1 $- 0.531$WL1 $+ 0.358$DLH4 $+ 0.340$WL3_2 $- 0.334$WL1_2
AE 1–6	0.893	0.798	0.771	30.035	$-28.2 + 0.325$WL3 $+ 0.171$WL2_1 $+ 0.177$WL3_2 $+ 0.321$DLH5 $- 0.330$WL1
AE 1–7	0.903	0.816	0.780	22.803	$-38.2 + 0.427$WL3 $+ 0.292$WL2_1 $+ 0.455$DLH1 $- 0.540$WL1 $+ 0.355$DLH4 $+ 0.359$WL3_2 $- 0.356$WL1_2
ACCAE	0.770	0.593	0.563	19.913	$15.0 + 0.943$WL3 $+ 1.040$DLH1 $- 0.921$WL1
Dependent Var.	R	R^2	R_a^2	F	Transfer Functions
DEF 4	0.524	0.275	0.258	16.686	$37.5 - 0.0875$WL2
DEF 5	0.757	0.573	0.553	28.858	$91.9 - 0.171$WL4 $- 0.131$DLH4_1
DEF 6	0.867	0.752	0.733	40.426	$114.1 - 0.277$DLH5 $- 0.0776$WL2_1 $- 0.0688$WL2_2
DEF 7	0.583	0.340	0.309	10.825	$82.6 - 0.304$WL2_1 $+ 0.255$WL1_1
DEF 4–5	0.711	0.506	0.483	22.023	$127.6 - 0.253$WL2 $- 0.133$DLH4_1
DEF 5–6	0.886	0.785	0.764	36.546	$202.4 - 0.209$WL2_1 $+ 0.288$WL1 $- 0.382$DLH4 $- 0.345$WL3
DEF 6–7	0.803	0.645	0.610	18.194	$198.0 - 0.293$WL4 $- 0.177$WL2_1 $- 0.344$DLH5 $+ 0.362$WL1
DEF 4–6	0.854	0.730	0.710	36.864	$255.2 - 0.351$WL4 $- 0.206$WL2_1 $- 0.404$DLH1
DEF 5–7	0.865	0.748	0.723	29.742	$279.7 - 0.459$WL4 $- 0.271$WL2_1 $- 0.360$DLH5 $+ 0.423$WL1
DEF 4–7	0.871	0.758	0.734	31.371	$357.3 - 0.629$WL4 $- 0.289$WL2_1 $- 0.683$DLH1 $+ 0.444$WL1
DEF 1–6	0.873	0.761	0.731	24.885	$261.3 - 0.379$WL4 $- 0.178$WL2_1 $+ 0.483$WL1 $- 0.453$DLH1 $- 0.338$DLH4
DEF 1–7	0.864	0.746	0.720	29.323	$362.2 - 0.657$WL4 $- 0.277$WL2_1 $+ 0.477$WL1 $- 0.683$DLH1
ACCDEF	0.819	0.671	0.647	27.826	$500.8 - 0.826$WL4 $+ 0.767$WL1 $- 1.142$DLH1

and up to 62.7% for periods longer than 3 months using the same regression analysis procedures. Only for the period from previous July to current June, the model of precipitation ($R_a^2 = 0.640$) outperforms that of AE (0.563) and RSM (0.380), while the model of DEF is still slightly better with $R_a^2 = 0.657$.

We also obtained the gridded PDSI data from a global data set for 1870–2002 (Dai *et al.*, 2004). Using the PDSI data of the four closest grids (36.25–38.75 °N, 95.25–98.75 °E) to Delingha, we estimated the PDSI values using tree-ring chronologies for the same set of monthly and seasonal combinations during the same calibration period of 1955–2002. In general, the regression models of the simulated soil moisture variables are better than those of the PDSI in most cases. For example, the best result of regression analysis for individual month was for June PDSI with $R_a^2 = 0.719$ as compared to $R_a^2 = 0.751$, 0.733, and 0.681 for June AE, DEF, and RSM, respectively. The best result for bi-monthly PDSI was for May–June PDSI with $R_a^2 = 0.710$ as compared to $R_a^2 = 0.800$, 0.764, and 0.749 for May–June AE, DEF, and RSM, respectively. The R_a^2 value for May–July PDSI was 0.717 as compared to $R_a^2 = 0.753$, 0.723, and 0.720 for May–July AE, DEF, and RSM, respectively. The improvements of the water balance variables over the PDSI, we believe, came from the capability of the model to adjust for local and regional characteristics. Based on the above results, we concluded that the simulated soil moisture variables can be reconstructed using tree-ring widths with the same or higher confidence as in the case of reconstruction of precipitation or PDSI in this region.

As mentioned above, the chronology at WL1 was allowed to enter the transfer models with opposite signs

DOI: 10.1002/joc

Table VI. (*Continued*).

Dependent Var.	R	R^2	R_a^2	F	Transfer Functions
RSM 4	0.762	0.581	0.539	13.838	−28.4 − 0.258WL1 + 0.414DLH1 + 0.107WL3_1 + 0.161WL3
RSM 5	0.838	0.701	0.671	22.906	−21.5 + 0.128WL2_1 + 0.167WL3_2 + 0.180WL3 − 0.151WL1_2
RSM 6	0.843	0.710	0.681	24.469	−17.2 + 0.245WL3 + 0.097WL2_1 − 0.317WL1 + 0.243DLH4
RSM 7	0.610	0.372	0.342	12.452	−1.10 + 0.100WL2_1 + 0.096WL4
RSM 4–5	0.810	0.655	0.620	18.541	−39.4 + 0.358DLH1 + 0.175WL3_2 − 0.163WL1_2 + 0.142WL3_1
RSM 5–6	0.882	0.778	0.749	27.274	−27.3 + 0.211WL3 + 0.117WL2_1 − 0.300WL1 + 0.197DLH1 + 0.147DLH4
RSM 6–7	0.776	0.602	0.562	15.134	−9.04 + 0.130WL4 + 0.102WL2_1 + 0.199DLH5 − 0.207WL1
RSM 4–6	0.860	0.739	0.713	28.352	−24.4 + 0.105WL2_1 + 0.266DLH1 − 0.216WL1 + 0.224WL3
RSM 5–7	0.867	0.752	0.720	23.601	−18.8 + 0.145WL4 + 0.099WL2_1 + 0.207DLH1 − 0.265WL1 + 0.123DLH4
RSM 4–7	0.865	0.749	0.723	29.766	−20.2 + 0.105WL2_1 + 0.238DLH1 + 0.194WL3 − 0.189WL1
RSM 1–6	0.775	0.601	0.561	15.056	−13.9 − 0.191WL1_1 + 0.241*DLH1 − 0.108WL2_1 + 0.136WL3_1
RSM 1–7	0.797	0.635	0.599	17.429	−12.1 + 0.116WL2_1 + 0.227DLH1 − 0.187WL1_1 + 0.124WL3_1
ACCRSM	0.650	0.422	0.380	9.972	3.4 + 0.163WL3 − 0.183WL1 + 0.156DLH1
RSM 5–6 RC	0.772	0.595	0.566	20.105	−34.2 + 0.2291 RC + 0.1344 RC_1 + 0.076 RC_2

Dependent Variables: AET, DEF and RSM are actual evapotranspiration, deficit, and relative soil moisture, respectively. The number denotes individual months or monthly combinations. ACC indicates the period from July of previous year to current June. RSM 5–6 RC is the model for May–June relative soil moisture based on the regional chronology.
Column headings: R, R^2, and $R_a{}^2$ are multiple correlation coefficients, coefficients of determination, and adjusted coefficients of determination of regression analysis, respectively. F is the F statistic for the statistical significance of the regression models.
Independent Variables: The letters represent the chronologies (Figure 3) and the numbers after underscore represent the lagged years.

Table VII. Results of principal component analysis (PCA) of the ring-width chronologies during the calibration period.

Eigenvalues of the correlation matrix: Total = 9 Average = 1				
PC	Eigenvalue	Difference	Proportion	Cumulative
1	7.226	6.709	0.803	0.803
2	0.516	0.140	0.057	0.860
3	0.377	0.024	0.042	0.902
4	0.353	0.153	0.039	0.941
5	0.199	0.078	0.022	0.963
6	0.121	0.039	0.014	0.977
7	0.082	0.013	0.009	0.986
8	0.069	0.013	0.008	0.994
9	0.056	–	0.006	1.000

Eigenvectors of the first 5 PCs					
Chronologies	PC1	PC2	PC3	PC4	PC5
DLH1	0.3064	0.3770	0.3856	0.7183	−0.1413
DLH2	0.3349	0.4301	0.2445	−0.2961	0.0136
DLH3	0.3383	0.3331	−0.0899	−0.4330	−0.0075
DLH4	0.3406	−0.0006	−0.4573	0.0111	0.3971
DLH5	0.3572	0.1270	0.0025	−0.1486	0.0981
WL1	0.3249	−0.0329	−0.6190	0.3884	−0.0760
WL2	0.3235	−0.4199	0.4243	0.0301	0.5656
WL3	0.3400	−0.2631	0.0592	−0.1868	−0.6758
WL4	0.3318	−0.5470	0.0875	0.0075	−0.1734

DOI: 10.1002/joc

Table VIII. Cross validation of the reconstructed series during the calibration period 1955–2002. The variables are the same as in Table VI for the transfer equations.

Variables	Sign test for the 1st Diff.	Sign test	Product mean *t*-value	Reduction of error	Correlation coefficient
AE 4	25	32**	3.73	0.38	0.62
AE 5	30*	35**	4.67	0.63	0.80
AE 6	37**	39**	5.11	0.72	0.85
AE 7	24	30*	2.41	0.29	0.55
AE 4–5	26	35**	5.19	0.59	0.77
AE 5–6	34**	39**	4.92	0.76	0.88
AE 6–7	29*	32**	4.67	0.60	0.78
AE 4–6	33**	40**	4.28	0.73	0.85
AE 5–7	32**	37**	4.27	0.71	0.84
AE 4–7	28	37**	4.40	0.72	0.85
AE 1–6	32**	40**	4.10	0.73	0.85
AE 1–7	28	38**	4.25	0.73	0.85
ACCAE	33**	36**	3.57	0.49	0.70
DEF 4	28	31*	1.82	0.20	0.46
DEF 5	33**	34**	4.52	0.51	0.71
DEF 6	30*	37**	4.45	0.71	0.84
DEF 7	20	27	3.63	0.24	0.50
DEF 4–5	24	32*	4.16	0.44	0.66
DEF 5–6	34**	38**	5.05	0.74	0.86
DEF 6–7	29*	34**	3.89	0.53	0.73
DEF 4–6	33**	38**	4.39	0.67	0.82
DEF 5–7	32**	37**	4.23	0.68	0.82
DEF 4–7	35**	37**	4.25	0.69	0.83
DEF 1–6	29*	36**	4.59	0.68	0.82
DEF 1–7	34**	38**	4.17	0.68	0.82
ACCDEF	29*	35**	4.21	0.59	0.77
RSM 4	20	33**	3.25	0.47	0.69
RSM 5	24	36**	4.53	0.60	0.78
RSM 6	32**	35**	4.65	0.64	0.80
RSM 7	26	28	2.52	0.24	0.50
RSM 4–5	25	33**	4.75	0.54	0.74
RSM 5–6	31**	35**	4.49	0.70	0.84
RSM 6–7	26	32**	3.85	0.54	0.74
RSM 4–6	27	37**	4.11	0.68	0.82
RSM 5–7	27	33**	4.22	0.67	0.82
RSM 4–7	28	35**	4.20	0.69	0.83
RSM 1–6	26	35**	4.00	0.49	0.70
RSM 1–7	26	36**	4.06	0.53	0.73
ACCRSM	24	32**	2.45	0.28	0.55
RSM56_ RC	33**	34**	4.72	0.48	0.69

Sign test results: *p ≤ 0.05, **p ≤ 0.01

to the other chronologies. We first noted this peculiarity when performing the stepwise regression where WL1 entered the models consistently with opposite signs. The site is located in the southeastern corner of the study area, with close proximity to WL2 (Figure 1). This chronology rendered the lowest correlations with the simulated soil moisture variables (Table V). However, it was strongly correlated with the chronologies at other sites ($R = 0.541–0.759$). To further investigate the relationship among the tree ring chronologies, we used principal component analysis (PCA), a data reduction procedure in which new variables (principal components or PCs), orthogonal to each other are constructed as linear combinations of the original variables. The new dataset normally has fewer variables, but contains most of the information in the original dataset (Johnston, 1978). Table VII presents the principal components (PC) eigenvalues and eigenvectors based on the data during the 1955–2001 calibration period. The first five PCs explained over 95% of the variance in the original dataset of nine tree-ring chronologies. It is interesting to note that the third PC demonstrated the contrast between WL1 and other chronologies, especially WL2 (although DLH4 had the same sign as WL1, but the magnitude was not as large). The two sites are very close spatially to each other but with quite different vegetation conditions. WL1 is on a south-facing slope of 35° to 40° steep, with thin and rocky soils and sparse Qilian junipers (Figure 2). WL2, on the other hand, is located inside a meandering river valley with probably the best moisture condition in the study area. During our visit to the site in late June 2005, the stream had a significant amount of runoff while almost all other streams of comparable size in the region were dry. It is the only site with Qinghai spruce as one of the dominant species and has the best canopy coverage among all sites (Figure 2). A closer look at the transfer functions in Table VI reveals that WL1 tends to coexist with WL2 (sometimes with 1 year lag) in the same equation. Of the 30 transfer equations in which various forms of WL1 are included, WL2 coexists for 24 of them. Perhaps it is the contrast between WL1 and WL2 that offered the additional explanation power in regression analysis.

We reconstructed all dependent variables listed in Table VI using the transfer equations. Besides the commonly used statistics in regression analysis, we also include indictors of the quality of the reconstructed series obtained by cross-validation, such as the results of sign test, sign test of first difference, and Student *t* test of product means, reduction of error, and correlation coefficients between the estimated and observed series (Fritts, 1976, 1991; Michaelsen, 1987). Based on the cross-validation of the transfer functions, we selected January–June AE (AE16), previous July – current June DEF (ACCDEF), and May–June RSM (RSM56) as the targets for reconstruction. All these variables have relatively good validation results (Table VIII) and represent different aspects of the soil moisture conditions. AE16 represents the thermal and moisture condition during the first half of the year prior to the peak of the growing season, ACCDEF represents the cumulative water shortage condition from the previous summer to the current growing season, and RSM56 represents soil moisture availability up to June, probably most critical to tree growth during the growing season. Figure 7 shows the actual and reconstructed values of these variables during the calibration period 1955–2002.

DOI: 10.1002/joc

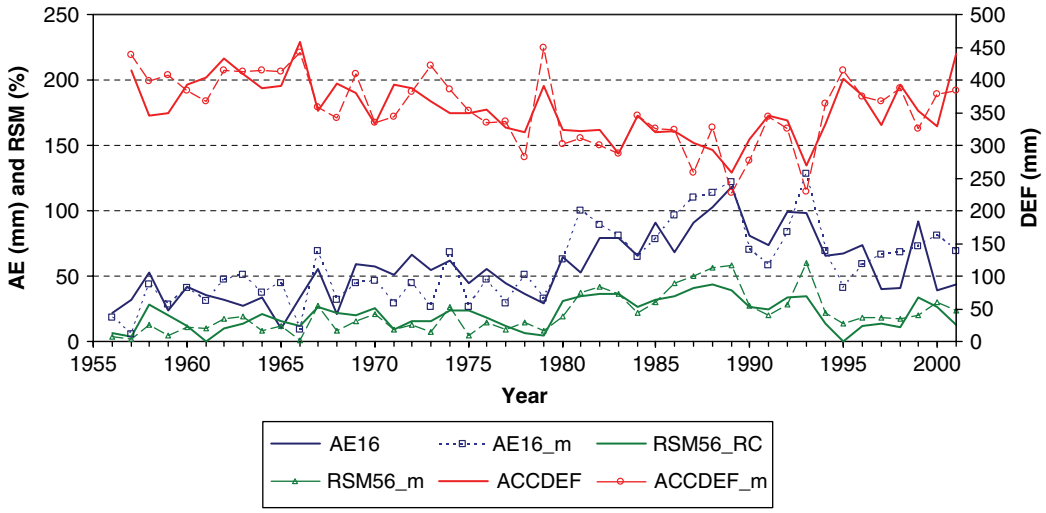

Figure 7. Reconstructed water balance variables (AE16, ACCDEF, and RSM56) plotted against the original values obtained from the model during 1955–2001. This figure is available in colour online at www.interscience.wiley.com/ijoc

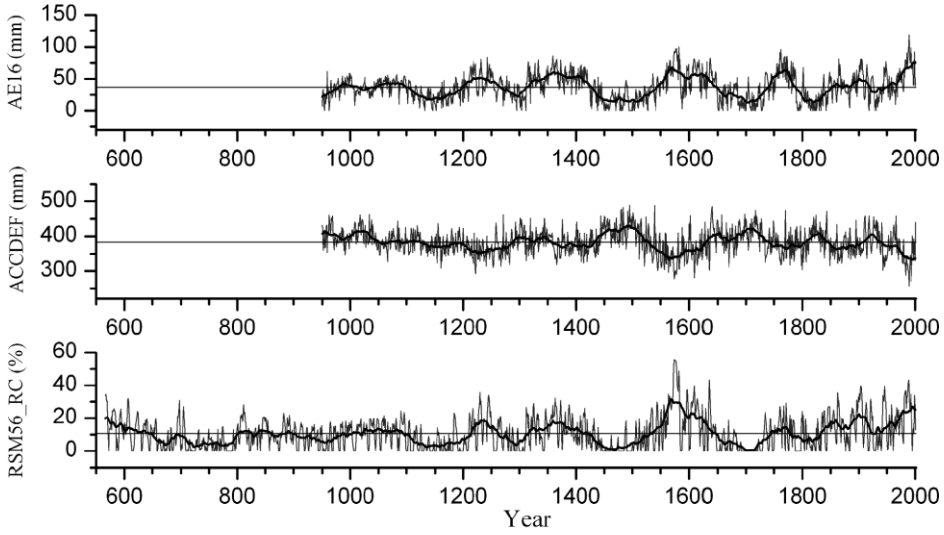

Figure 8. Reconstructed AE16 and ACCDEF series based on individual tree ring chronologies going back to 950 AD and the RSM56 series based on the regional chronology (RC) going back to 566 AD.

4.5. Regional moisture conditions in the past

Figure 8 displays the reconstructed records of soil moisture variables. For AE16 and ACCDEF, we reconstructed a record going back to 950 AD using the transfer models in Table VI. For RSM56, we reconstructed a longer series using the RC, which goes back to 566 AD. After passing a 31-year moving average filter to the time-series, significant low-frequency variation patterns can be seen, including prominent dry periods during 700–800 AD, 1100–1200 AD, 1425–1525 AD, and 1650–1750 AD, wet periods around 1225 AD, 1350 AD, and 1525–1650 AD, and a general trend toward a wetter condition during the most recent 300 years. The recent trend to a wetter condition conformed to the ice accumulation record during 1600–1980 based on the ice core taken from the Dunde Glacier (38°06′N, 96°24′E, 5325 m) northwest of the study region (Thompson *et al*., 1995). The wetter trend was also corroborated by a recent study in northern Pakistan, in which a reconstructed precipitation record based on tree-ring data indicated that the 20th Century was the wettest period during the past millennium (Treydte *et al*., 2006).

There are several published series of proxies of climatic variation for the Qinghai Lake (Figure 1), the largest closed inland saline lake in China whose salinity and water level are closely related to the freshwater input. A 900 year record of salinity of the Qinghai Lake was obtained from the microfossils of ostracoda (seed shrimp) of Crustacea from the sediment cores (Zhang *et al*., 2004b). More specifically, paleosalinity of the lake water was reconstructed based on the length of *Limnocythere inopinata* and the Sr/Ca ratio in the shells of *Eucypris inflata*. Additionally, we compared the reconstructed moisture conditions to approximately 800 year

DOI: 10.1002/joc

records of the percentage of coarse particles (>63 μm) and oxygen stable isotope in carbonate salts in the lake sediments (Zhang *et al.*, 2003b), with the assumptions that years with more freshwater input would also saw greater accumulation of coarse sediment particles and that the oxygen isotope is related to the regional effective precipitation. A comparison with the reconstructed moisture conditions confirmed the dampened fluctuations during the period before 1500, while greater high-frequency and low-frequency variations were apparent during the Little Ice Age (Figure 9).

We used decadal averages in the comparisons between the salinity and sedimentary data of the Qinghai Lake and the reconstructed moisture conditions. We found that ACCDEF and AE16 were significantly correlated with the salinity, but not with the coarse particle percentage and stable isotope records during the entire periods with available data (Table IX). Figure 9 also shows that for the most recent 400 years, there are probably stronger associations between the Qinghai Lake data and the reconstructed moisture conditions. We found statistically significant correlations between the oxygen stable isotope and reconstructed moisture variables during the periods since 1600, 1700, and 1800 respectively, but no significant correlation was found for the percentage of coarse particles (Table IX). Particle size may represent some complex physical processes since it is influenced by both total precipitation and rainfall intensity. It is also influenced by the seasonality of the rainfall events and the mixing mechanisms in the lake. For example, a single heavy rainfall event occurring in the early summer before vegetation is fully established may generate more coarse sediment particles than a similar event occurring into the summer season or many low-intensity long-duration rainfall events distributed throughout the summer season. There are obvious differences between the reconstructed moisture variables and other proxies of precipitation. The close relationships between the moisture variables and the tree ring chronologies (Tables V and VI) indicate that these reconstructed variables reflect the climate variability from different perspectives than those proxies compared here.

5. Conclusions

During the period of 1998–2003, we collected a total of 1050 increment cores out of 493 Qilian junipers in the Delingha region of Qinghai Province, northeastern Qaidam Basin, to construct chronologies of approximately 800–1500 years long at eleven sampling sites. Using the Thornthwaite–Mather water balance model, we generated variables to represent soil moisture and vegetation water use conditions. The modelling process combines the effects of both temperature and precipitation variations and simulates the soil moisture depletion process. As a result, the relationships between tree-ring widths and the simulated soil moisture variables were found typically better than those between tree-ring widths and precipitation or temperature. The simulated soil moisture variables also produced better results than PDSI. By considering spatial variation patterns of topography and soil properties, water balance modelling may further help explain inter-site variations and separate local and regional climate signals in the tree-ring samples. The result of simulation based on meteorological data during 1955–2002 showed significant interannual variability

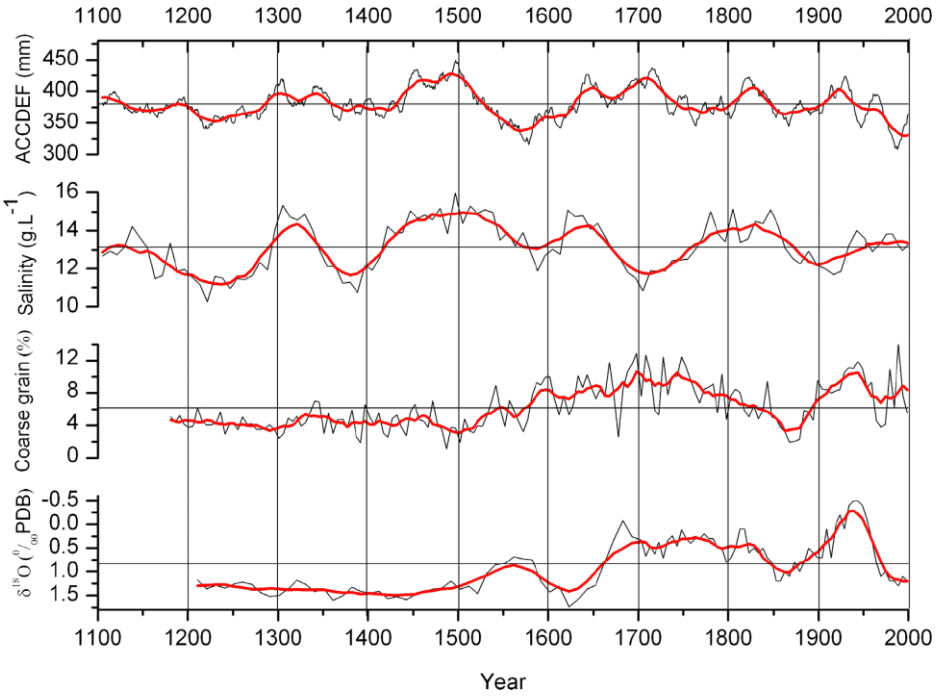

Figure 9. A comparison between the reconstructed ACCDEF (10 year moving averages), salinity, percentage of coarse particles in lake sediment, and oxygen stable isotope in carbonate salts of the Qinghai Lake. This figure is available in colour online at www.interscience.wiley.com/ijoc

DOI: 10.1002/joc

Table IX. Spearman's rank correlation coefficients between Qinghai Lake salinity, percentage of coarse sediment (>63 m), sediment stable oxygen isotope and the reconstructed moisture conditions. Boldface numbers indicate statistical significance of 0.05.

	Moisture Variables		Grain Size (% <63 μm)	δ^{18}O (‰ PDB)	Salinity (g/l)
All decades	ACCDEF	Correlation Coefficient	−0.004	0.043	**0.252**
		Sig. (2-tailed)	0.968	0.710	0.017
		N	82	79	90
	AE16	Correlation Coefficient	0.057	0.082	**−0.241**
		Sig. (2-tailed)	0.610	0.471	0.022
		N	82	79	90
	RSM56	Correlation Coefficient	0.083	−0.007	−0.125
		Sig. (2-tailed)	0.460	0.953	0.240
		N	82	79	90
Since 1600	ACCDEF	Correlation Coefficient	0.189	−0.274	−0.258
		Sig. (2-tailed)	0.243	0.087	0.107
		N	40	40	40
	AE16	Correlation Coefficient	0.006	0.288	0.110
		Sig. (2-tailed)	0.970	0.071	0.498
		N	40	40	40
	RSM56	Correlation Coefficient	−0.191	**0.401**	0.204
		Sig. (2-tailed)	0.237	0.010	0.206
		N	40	40	40
Since 1700	ACCDEF	Correlation Coefficient	0.039	−0.348	−0.348
		Sig. (2-tailed)	0.838	0.059	0.060
		N	30	30	30
	AE16	Correlation Coefficient	0.136	0.115	0.028
		Sig. (2-tailed)	0.472	0.543	0.885
		N	30	30	30
	RSM56	Correlation Coefficient	−0.162	**0.400**	0.182
		Sig. (2-tailed)	0.393	0.028	0.335
		N	30	30	30
Since 1800	ACCDEF	Correlation Coefficient	−0.087	**−0.589**	−0.155
		Sig. (2-tailed)	0.715	0.006	0.514
		N	20	20	20
	AE16	Correlation Coefficient	0.158	**0.499**	−0.317
		Sig. (2-tailed)	0.506	0.025	0.173
		N	20	20	20
	RSM56_RC	Correlation Coefficient	0.096	**0.481**	−0.147
		Sig. (2-tailed)	0.686	0.032	0.535
		N	20	20	20

in soil moisture conditions in the study area. We found strong correlations between the tree-ring widths and the simulated soil moisture variables for individual months as well as for various bi-monthly and seasonal time periods. Correlation and regression analyses also revealed the lagged effect of soil moisture on tree growth. Generally speaking, actual evapotranspiration (AE) produced the best results in reconstruction, followed by deficit (DEF) as a measure of water use stress.

The reconstructed records of the soil moisture variables displayed significant fluctuation patterns during the past 1400 years, which may not have been revealed by examining precipitation or temperature records alone. We were able to identify extended periods of significant dry and wet anomalies. After comparing with other proxies of climate variation in the study region, including ice core, lake water salinity, percentage of coarse sediment and oxygen stable isotope in carbonate salts, we concluded that the reconstructed moisture variables corroborated well with existing proxies of past precipitation and most likely provided additional information of the climate variation patterns in the region. Our results suggest that water balance modelling offers great potential in reconstruction of paleoenvironments at the interannual to interdecadal scales.

Acknowledgements

This study was in part supported by grants from NASA (EOS/03–0063–0069), Chinese Academy of Sciences (KZCX3–SW–339), K.C. Wang Education Foundation of Hong Kong (2005), and University of San Diego (FRG 05–06 and 06–07). The authors would like to thank Dr Enlou Zhang of the Nanjing Institute of Geography

DOI: 10.1002/joc

and Limnology, Chinese Academy of Sciences, and Prof. Fahu Chen and Dr Jiawu Zhang of Lanzhou University, who graciously provided the paleosalinity and sedimentary data of the Qinghai Lake. Thanks also to the anonymous reviewer who provided valuable constructive suggestions and comments.

References

Bradley RS. 1999. *Paleoclimatology: Reconstructing Climates of the Quaternary*, 2nd edn. Academic Press: New York; 613.

Bradley RS. 2000. Past global changes and their significance for the future. *Quaternary Science Reviews* **19**: 391–402.

Bradley RS, Hughes MK, Diaz HF. 2003. Climate in medieval time. *Science* **302**(5644): 404–405.

Briffa KR, Osborn TJ. 1999. Climate warming: seeing the wood from the trees. *Science* **284**(5416): 926–927.

Buckley BM, Cook ER, Wilson RJS, Kelly PE, Larson DW. 2004. Inferred summer precipitation for southern Ontario back to AD 610, as reconstructed from ring widths of Thuja occidentalis. *Canadian Journal of Forest Research* **34**(12): 2541–2553.

Cook ER, Kairiukstis LA. 1990. *Methods of Dendrochronology: Applications in the Environmental Sciences*. Kluwer, Academic Publishers for International Institute for Applied Systems Analysis: Dordercht/Boston/London 394.

Cook ER, Woodhouse CA, Eakin CM, Meko DM, Stahle DW. 2004. Long-term aridity changes in the western United States. *Science* **306**: 1015–1018.

Dai A, Trenberth KE, Qian T. 2004. A global data set of Palmer drought severity index for 1870–2002: relationship with soil moisture and effects of surface warming. *Journal of Hydrometeorology* **5**: 1117–1130.

Du Q, Sun SZ. 1990. *Vegetation in the Chaidamu (Qaidam) Basin Region and its Utilization* (in Chinese). Science Press: Beijing; 129.

Dunne T, Leopold LB. 1978. *Water in Environmental Planning*. W.H. Freeman and Company: New York; 810.

Feddema JJ. 1998. Estimated impacts of soil degradation on the African water balance and climate. *Climate Research* **10**(2): 127–141.

Feddema JJ. 1999. Future African water resources: interactions between soil degradation and global warming. *Climatic Change* **42**(3): 561–596.

Folland CK, Karl TR, Christy JR, Clarke RA, Gruza GV, Jouzel J, Mann ME, Oerlemans J, Salinger MJ, Wang S-W. 2001. Observed climate variability and change. In *IPCC Third Assessment Report – Climate Change 2001: The Scientific Basis*. Intergovernmental Panel on Climate Change (IPCC), World Meteorological Organization/UNEP: New York; 99–182.

Fritts HC. 1976. *Tree Rings and Climate*. Academic Press: London; 567.

Fritts HC. 1991. *Reconstructing Large-Scale Climatic Patterns from Tree-Ring Date – A Diagnostic Analysis*. University of Arizona Press: Tucson, Arizona; 286.

Hidalgo HG. 2004. Climate precursors of multidecadal drought variability in the western United States. *Water Resources Research* **40**(12): 1–10.

Hodny JW, Mather JR. 1999. Climate change and water resources of the delaware river basin. *The Pennsylvania Geographer* **37**(2): 3–19.

Holmes RL. 1983. Computer-assisted quality control in tree-ring dating and measurement. *Tree-Ring Bulletin* **43**: 69–78.

Hughes MK, Funkhouser G. 2003. Frequency-dependent climate signal in upper and lower forest border tree rings in the mountains of the Great Basin. *Climatic Change* **59**(1–2): 233–244.

Hughes MK, Funkhouser G, Vaganov EA, Shiyatov S, Touchan R. 1999. Twentieth-century summer warmth in northern Yakutia in a 600-year context. *Holocene* **9**(5): 629–634.

Hulme M, Marsh R, Jones PD. 1992. Global changes in a humidity index between 1931–60 and 1961–90. *Climate Research* **2**(1): 1–22.

Johnston RJ. 1978. *Multivariate Statistical Analysis in Geography: A Primer on the General Linear Model*. Longman: London; 280.

Kang XC, Graumlich LJ, Sheppard PR. 1997. A 1835-year tree-ring chronology and its preliminary analysis in Dulan region, Qinghai. *Chinese Science Bulletin* **42**(13): 1122–1124.

Kenny GJ, Harrison PA. 1992. Thermal and moisture limits of grain maize in Europe: model testing and sensitivity to climate change. *Climate Research* **2**(2): 113–129.

Kirchhefer AJ. 2001. Reconstructions of summer temperatures from tree-rings of Scots pine (*Pinus sylvestris L.*) in coastal northern Norway. *Holocene* **11**(1): 41–52.

Lamb HH. 1995. *Climate, History and the Modern World*, 2nd edn. Roughtledge: London; 433.

Leathers DJ, Grundstein AJ, Ellis AW. 2000. Growing season moisture deficits across the northeastern United States. *Climate Research* **14**(1): 43–55.

Leavitt SW. 2002. Prospects for reconstruction of seasonal environment from tree-ring δ 13C: baseline findings from the Great Lakes area, USA. *Chemical Geology* **192**(12): 47–58.

LeBlanc D, Terrella M. 2001. Dendroclimatic analyses using Thornthwaite – Mather – type evapotranspiration models: a bridge between dendroecology and forest simulation models. *Tree-Ring Research* **57**(1): 55–66.

Mather JR. 1978. *The Climatic Water Balance in Environmental Analysis*. D.C. Heath and Company: Lexington, MA; 239.

Meentemeyer V, Gardner J, Box EO. 1985. World patterns and amounts of detrital soil carbon. *Earth Surface Processes and Landforms* **10**(6): 557–567.

Meko D, Hughes MK, Cook ER, Stahle DW, Stockton CW. 1993. Spatial patterns of tree-growth anomalies in the United States and southeastern Canada. *Journal of Climate* **6**(9): 1773–1786.

Meko DM, Woodhouse CA. 2005. Tree-ring footprint of joint hydrologic drought in Sacramento and upper Colorado river basins, western USA. *Journal of Hydrology* **308**(1–4): 196–213.

Michaelsen J. 1987. Cross-validation in statistical climate forecast models. *Journal of Climate and Applied Meteorology* **26**: 1589–1600.

Piutti E, Cescatti A. 1997. A quantitative analysis of the interactions between climatic response and intraspecific competition in European beech. *Canadian Journal of Forestry Research* **27**: 277–284.

Puckett LJ. 1981. *Dendroclimatic Estimates of a Drought Index for Northern Virginia*. U.S. Geological Survey: Water-Supply Papers 2080, Government Printing Office: Washington, DC 39.

Robertson EO, Jozsa LA, Spittlehouse DL. 1990. Estimating douglas-fir wood production from soil and climate data. *Canadian Journal of Forest Research* **20**(3): 357–364.

Rosenberg NJ, Blad BL, Verma SB. 1983. *Microclimate: The Biological Environment*, 2nd edn. Wiley: New York; 495.

Shabalova MV, van Deursen WPA, Buishand TA. 2003. Assessing future discharge of the river Rhine using regional climate model integrations and a hydrological model. *Climate Research* **23**(3): 233–246.

Shao X, Fang X, Liu H, Huang L. 2003. Dating the 1000-year old Qilian juniper from mountains of the eastern extreme of the Qaidam Basin. *Acta Geographica Sinica (in Chinese)* **58**: 90–100.

Shao X, Huang L, Liu H, Liang E, Fang X, Wang L. 2005. Reconstruction of precipitation variation from tree rings in recent 1000 years in Delingha, Qinghai. *Science in China Series D Earth Sciences* **48**: 939–949.

Sharma KP, Vorosmarty CJ, Moore B III. 2000. Sensitivity of the Himalayan hydrology to land-use and climatic changes. *Climatic Change* **47**(1–2): 117–139.

Sheppard PR, Hughes MK, Comrie AC, Packin GD, Angersbach K. 2002. The climate of the US Southwest. *Climate Research* **21**(3): 219–238.

Sheppard PR, Tarasov PE, Graumlich LJ, Heussner K-U, Wagner M, Osterle H, Thompson LG. 2004. Annual precipitation since 515 BC reconstructed from living and fossil juniper growth of northeastern Qinghai Province, China. *Climate Dynamics* **23**: 869–881.

Tarasov P, Heussner K-U, Wagner M, Wang S. 2003. Precipitation changes in Dulan 515 BC – 800 AD inferred from tree ring data related to the human occupation of NW China. *Eurasia Antiqua Band* **9**: 303–321.

Tardif J, Brisson J, Bergeron Y. 2001. Dendroclimatic analysis of Acer saccharum, *Fagus grandifolia*, and *Tsuga canadensis* from an old-growth forest, southwestern Quebec. *Canadian Journal of Forest Research* **31**(9): 1491–1501.

Taylor AH, Beaty RM. 2005. Climatic influences on fire regimes in the northern Sierra Nevada Mountains, Lake Tahoe Basin, Nevada, USA. *Journal of Biogeography* **32**(3): 425–438.

Thompson LG, Mosley-Thompson E, Dansgaard W, Grootes PM. 1986. The little ice age as recorded in the stratigraphy of the tropical Quelccaya Ice cap. *Science* **234**: 361–364.

Thompson LG, Mosley-Thompson E, Davis ME. 1995. A 1000 year climate ice-core record from the Guliya ice cap, China: its relationship to global climate variability. *Annals of Glaciology* **21**: 175–181.

DOI: 10.1002/joc

Thompson LG, Mosley-Thompson E, Davis ME, Lin N, Yao T, Dyurgerov M, Dai J. 1993. Recent warming: ice core evidence from tropical ice cores, with emphasis on central Asia. *Global and Planetary Change* **7**: 145–156.

Thornthwaite CW, Mather JR. 1957. *Instructions and Tables for Computing Potential Evapotranspiration and the Water Balance*. Drexel Institute of Technology, Laboratory of Climatology: *Publications in Climatology*, Vol. 10(3). Centerton, NJ; 311.

Treydte KS, Schelser GH, Helle G, Frank DC, Winiger M, Haug GH, Esper J. 2006. The twentieth century was the wettest period in northern Pakistan over the past millennium. *Nature* **440**: 1179–1182 DOI: 10.1038.

Wang J. 1993. Qilian juniper. In *Qinghai Forest*, Editing Committee of Qinghai Forest (ed.). Chinese Forestry Publishing House (in Chinese): Beijing, China; 230–240.

Wigley TML, Briffa KR, Jones PD. 1984. On the average value of correlated time series, with applications in dendroclimatology and hydrometeorology. *Journal of Climate and Applied Meteorology* **23**: 201–213.

Woodhouse CA. 2001. A tree-ring reconstruction of streamflow for the Colorado front range. *Journal of the American Water Resources Association* **37**(3): 561–569.

Yang B, Achim B, Shi Y, Chen F. 2004. Evidence for a late Holocene warm and humid climate period and environmental characteristics in the arid zones of northwest China during 2.2 ∼ 1.8 kyr B.P. *Journal of Geophysical Research D – Atmospheres* **109**(2): D02105 1–10.

Zhang Z, Mann ME, Cook ER. 2004a. Alternative methods of proxy-based climate field to reconstruction: application to summer drought over conterminous United States back to AD 1700 from tree-ring data. *Holocene* **14**(4): 502–516.

Zhang E, Shen J, Wang S, Yin Y, Zhu Y, Xia W. 2004b. Quantitative reconstruction of the paleosalinity at Qinghai Lake in the past 900 years. *Chinese Science Bulletin* **49**(7): 730–734.

Zhang Q-B, Cheng G, Yao T, Kang X, Huang J. 2003a. A 2,326-year tree-ring record of climate variability on the northeastern Qinghai-Tibetan plateau. *Geophysical Research Letters* **30**(14): DOI: 10.1029/2003GL017425.

Zhang J, Jin M, Chen F, Battarbee RW, Henderson ACG. 2003b. High-resolution precipitation variations in the Northeast Tibetan Plateau over the last 800 years documented by sediment cores of Qinghai Lake. *Chinese Science Bulletin* **48**(14): 1451–1456.

Zheng D. 1996. The system of physico-geographical regions of the Qinghai-Xizang (Tibet) plateau. *Science in China. Series D* **39**(4): 410–417.